

Impact of the spatiotemporal variability of the nutrient flux on primary productivity in the ocean

C. Pasquero

Geological and Planetary Sciences Division, California Institute of Technology, Pasadena, California, USA

A. Bracco

Physics of Weather and Climate Group, Abdus Salam International Center for Theoretical Physics, Trieste, Italy

A. Provenzale

Istituto di Scienze dell'Atmosfera e del Clima, Consiglio Nazionale delle Ricerche, Torino, Italy

Received 1 October 2004; revised 24 March 2005; accepted 11 April 2005; published 8 July 2005.

[1] Oceanic carbon uptake depends on the productivity of the marine ecosystem. Here we study the dependence of primary productivity on the spatial and temporal variability of the nutrient flux and the functional form used to parameterize it. We show that primary productivity is significantly affected by the form of the nutrient input. For a restoring flux, used to parameterize nutrient input by upwelling, primary productivity depends on the size and/or temporal duration of the upwelling events. For a fixed-flux nutrient input, we show that high-nutrient, low-chlorophyll (HNLC) regions can easily appear, without necessarily implying the lack of some micronutrient. These results have interesting implications on the interpretation of primary productivity estimates from observational data and ocean circulation models, and indicate a way to obtain upper and lower bounds to primary productivity in coarse-resolution models.

Citation: Pasquero, C., A. Bracco, and A. Provenzale (2005), Impact of the spatiotemporal variability of the nutrient flux on primary productivity in the ocean, *J. Geophys. Res.*, 110, C07005, doi:10.1029/2004JC002738.

1. Introduction

[2] Planktonic growth and the related carbon dioxide uptake from the atmosphere require the availability of several nutrients, which have to be supplied to the surface mixed layer to balance biological consumption and sinking of organic matter into deeper water. Depending on the geographical region, the season, and the type of nutrient considered, input fluxes can be driven by different physical processes, such as isopycnal and diapycnal diffusion, Ekman pumping, mixed layer deepening below the nutricline level, convection, aeolian deposition, sea-ice melting, transport from the boundaries, and biogenic fixation (see the reviews by Gargett and Marra [2002] and Williams and Follows [2003]).

[3] As first suggested by Jenkins [1988] in an analysis of plankton dynamics in the Bermuda region, mesoscale and sub-mesoscale processes play an especially important role in determining the properties of nutrient input into the euphotic region. Eddy-pumping [Falkowski *et al.*, 1991; McGillicuddy and Robinson, 1997; Oschlies and Garcon, 1998; Siegel *et al.*, 1999], frontal region circulation [Mahadevan and Archer, 2000; Lévy *et al.*, 2001; Martin *et al.*, 2001], and strong diapycnal mixing associated with western boundary currents [Jenkins and Doney, 2003] are all examples of mesoscale and sub-mesoscale processes that

contribute to the nutrient supply into the surface mixed layer. Abraham [1998] and, more recently, Lévy and Klein [2004] have shown that mesoscale variability can play an important role also in explaining the spectral variability of phyto- and zoo-plankton populations. Martin *et al.* [2002] have shown that small upwelling regions associated with coherent vortices have strong effects on primary productivity in the open ocean. In a study of the isotopic concentration of nitrogen in the North Atlantic subtropical gyre, Mahaffey *et al.* [2004] conclude that the largest nitrogen input into the central region of the gyre is upward transported, deep-ocean nitrate and argue that phytoplankton are able to respond to transient, episodic, mesoscale injections of nutrients. Finally, the recent study on model intercomparison reported by Doney *et al.* [2004] confirms the sensitivity of carbon flux estimates to the presence of mesoscale flow structures.

[4] In this paper, we investigate the effects of the spatial and temporal variability of the nutrient input on plankton population dynamics and oceanic primary productivity. To this end, we use a simple nutrient-phytoplankton-zooplankton (NPZ) model and consider two types of nutrient input, representing, respectively, (1) mixing between nutrient-rich deep water and the mixed layer and (2) the effect of external nutrient sources such as wind-driven dust deposition. Horizontal advection is provided by barotropic turbulence, which we use as a first approximation to mesoscale turbulence in the open ocean. The present study extends and completes the results of Martin *et al.* [2002]. Here we consider the effect of using different functional forms for

the nutrient input, discuss in detail the physical and biological mechanisms which are responsible for the observed behavior, and suggest a way to estimate upper and lower bounds to primary productivity in coarse-resolution models.

[5] The NPZ model is described in section 2. In section 3 we investigate the response of a homogeneous NPZ ecosystem model to a prescribed time-dependent nutrient flux. In section 4 we consider the effects of advection and stirring, embedding the ecosystem dynamics in a two-dimensional turbulent flow. A discussion of the results and of their implications is given in section 5. In Appendix A we describe the semi-Lagrangian method used for integrating the NPZ model.

2. Nutrient-Phytoplankton-Zooplankton Dynamics

[6] We use one of the standard formulations of NPZ dynamics, where nutrient (N), phytoplankton (P), and zooplankton (Z) variables represent averaged concentrations in the surface mixed layer [Fasham *et al.*, 1990; Oschlies and Garcon, 1999; Martin *et al.*, 2002],

$$\begin{cases} \frac{dN}{dt} = f(N, P, Z) \equiv \Phi_N - \beta \frac{N}{k_N + N} P \\ \quad \quad \quad + \mu_N \left((1 - \gamma) \frac{a\epsilon P^2}{a + \epsilon P^2} Z + \mu_P P + \mu_Z Z^2 \right), \\ \frac{dP}{dt} = g(N, P, Z) \equiv \beta \frac{N}{k_N + N} P - \frac{a\epsilon P^2}{a + \epsilon P^2} Z - \mu_P P, \\ \frac{dZ}{dt} = h(N, P, Z) \equiv \gamma \frac{a\epsilon P^2}{a + \epsilon P^2} Z - \mu_Z Z^2. \end{cases} \quad (1)$$

[7] The terms on the right-hand side of the equation for the nutrient represent, respectively, vertical nutrient supply (e.g., due to upwelling or deposition), conversion of nutrient into organic matter through phytoplankton activity, and regeneration of the dead organic matter into nutrients. The only significant sink of nutrient is due to consumption by phytoplankton, consistent with the fact that nutrient downwelling typically occurs in nutrient-depleted regions, and the associated removal effect is correspondingly small. Phytoplankton dynamics is regulated by production, depending on available nutrients, through a Holling type II functional response, grazing by zooplankton, through a Holling type III functional response, and linear mortality (see e.g., Kot [2001] for a discussion of the Holling-type functional forms). Finally, zooplankton grow when phytoplankton are present (γ is the assimilation efficiency of the zooplankton), and a quadratic mortality term is used to close the system and to parameterize the effects of higher trophic levels. A nonlinear zooplankton mortality term has been shown to reduce the occurrence of oscillations introduced by nonlinear grazing [Steele and Henderson, 1992; Truscott and Brindley, 1994; Edwards and Yool, 2000]. In the present model, we do not include terms representing changes in plankton concentration due to vertical advection and mixing. The inclusion of these terms does not qualitatively affect the results as long as the average rate of change of plankton concentration due to vertical mixing is smaller than the plankton growth rate. The regeneration

Table 1. List of Parameters Used in the Ecosystem Model

Symbol	Value
β	0.66 day ⁻¹
ϵ	1.0 (mmol N m ⁻³) ⁻² d ⁻¹
γ	0.75
a	2.0 day ⁻¹
S	$S_n = 0.00648$ day ⁻¹ in nutrient-poor regions
S_a	$S_a = 0.648$ day ⁻¹ in nutrient-rich regions
k_N	0.5 mmol N m ⁻³
μ_N	0.2
μ_P	0.03 day ⁻¹
μ_Z	0.2 (mmol N m ⁻³) ⁻¹ d ⁻¹

efficiency, μ_N , is smaller than 1, and it represents the fact the not all biological substance is immediately available as nutrient: The fraction $(1 - \mu_N)$ is lost by detritus sinking to deeper water. Note that nutrient enters this model by affecting the growth rate of phytoplankton and that the model does not account for light dependence of phytoplankton dynamics. Since in this model we do not explicitly consider the vertical coordinate, any representation of light limitation on phytoplankton growth would be rather artificial. The parameter values used in the model are listed in Table 1, and they are typical of midlatitude subeuphotic concentrations [Fasham, 1993; Oschlies and Garcon, 1998]. Focusing on nitrate as the main nutrient, we define primary productivity (PP) as

$$PP = \beta \frac{N}{k_N + N} P. \quad (2)$$

This accounts for both the new production, fueled by newly available nutrient, and the production on regenerated matter.

[8] In the simple model considered here, N represents a general nutrient concentration and it can be any form of macro-nutrient (as nitrate, phosphate, silicate) or micro-nutrient (e.g., iron) limiting phytoplankton growth. Since no vertical structure of the fields is allowed, nutrient input into the mixed layer has to be parameterized. Mixing and advection processes between the nutrient-rich deep water and the mixed-layer water can be represented by a restoring flux (RF), where the concentration of nutrient at the surface relaxes to a value that depends on the (constant and large) nutrient content in the deep reservoir, N_0 :

$$\Phi_N = S(\mathbf{x}, t)(N_0 - N). \quad (3)$$

The relaxation time $1/S$ is a function of space and time and it measures the rate at which the nutrient relaxes to the value N_0 . With a restoring nutrient flux, the net nutrient input into the system depends on both the value of the relaxation rate, S , and the consumption by phytoplankton, which decreases the value of N with respect to N_0 . This form of the nutrient flux can also be interpreted as the finite difference approximation to a vertical advective term that acts between two layers with different nutrient concentration N and N_0 , and it is the standard formulation used for chemostat models when the reservoir has infinite capacity [Kot, 2001].

[9] External nutrient input processes, such as wind-driven dust deposition, are better represented by a nutrient

flux that does not depend on the nutrient content in the mixed layer,

$$\Phi_N = \Phi_0(\mathbf{x}, t). \quad (4)$$

This type of nutrient flux can also display spatiotemporal variability, and it will be referred to as fixed-flux (FF), to stress its independence of the surface nutrient concentration.

[10] With the choice of parameter values adopted here, in spatially homogeneous conditions and for a constant nutrient input, the NPZ model has only one nontrivial stable fixed point and no time-dependent asymptotic solutions, regardless of the specific functional form chosen for the nutrient supply (i.e., equation (3) or (4)). Different choices of parameter values lead to different homogeneous solutions, and, in some cases, to the appearance of limit cycles [e.g., *Truscott and Brindley, 1994; Edwards and Brindley, 1996*]. In this paper, we do not explore the parameter dependence of the homogeneous ecosystem solutions, and we concentrate on the effects of the spatial and temporal variability of the nutrient supply and on the role of horizontal advection when the homogeneous asymptotic solution of the ecosystem model is a stable fixed point.

3. Temporal Variability in Nutrient Supply

[11] Here we analyze the response of a homogeneous NPZ ecosystem model to a time-dependent nutrient flux, with no contribution from spatial inhomogeneities and advection. The results obtained in this section provide a guideline to interpret the behavior of the spatially inhomogeneous ecosystem, discussed in section 4.

3.1. Restoring Nutrient Flux

[12] First we consider the case of a restoring nutrient flux: The nutrient concentration in the surface mixed layer relaxes, with timescale $1/S$, to the constant deep-water nutrient concentration N_0 . To introduce temporal variability, we assume that the relaxation rate S varies periodically, and it takes two different values S_a and S_n , with $S_a \gg S_n$. The period of the fluctuation is T , and the relaxation rate is fixed at $S = S_a$ during the time interval T_a and at $S = S_n$ during the interval $T_n = T - T_a$. When $S = S_n$, the system is in “normal” conditions with weak nutrient input (due to slow relaxation to deep water values). During “active” phases, the relaxation rate becomes large, $S = S_a$, owing to the presence of strong vertical advection and upwelling, and the large supply of nutrient allows for the establishment of a large planktonic population.

[13] In the following, we explore the ecosystem response to a variation in the duration of the active and normal phases, and we ask whether primary productivity is sensitive to the duration of individual upwelling episodes (i.e., to the periodicity of the alternance between active and normal conditions), even if the total fraction of time during which the system experiences strong upwelling is kept constant.

[14] We integrate the NPZ model starting from equilibrium conditions (with $S = S_n$), and we turn on the periodic variation in the value of S . After an initial transient, the system settles into an oscillatory state with the same periodicity, T , of the nutrient variability. In Figure 1 we show the time evolution of N , P , Z and of the primary productivity, PP , for three examples with $T_a/T = 0.12$ and $T_a = 0.68d$, $T_a = 6.8d$ and $T_a =$

$136d$, respectively. When an active period starts, the nutrient concentration rapidly increases (see Figure 1, left) owing to the large nutrient flux, $S_a(N_0 - N)$, associated with the short relaxation time S_a^{-1} and the large difference $(N_0 - N)$. As N increases, the flux decreases because of the reduced difference $(N_0 - N)$. At the end of an active period, the nutrient flux first decreases, as a consequence of the larger relaxation time S_n^{-1} . During the following period of normal conditions, the nutrient concentration decreases owing to consumption by phytoplankton. As a consequence, the nutrient flux slowly increases again, owing to the increased difference $(N_0 - N)$ when N is reduced.

[15] In Figure 2a we show the mean primary productivity (averaged over one period T) as a function of the duration of the upwelling episodes, T_a , for a fixed value of the ratio T_a/T . Different lines correspond to different values of this ratio. As the ratio T_a/T increases, the system experiences a larger nutrient flux and therefore has larger primary productivity. More interestingly, when T_a/T is kept constant but the duration T_a of the individual events (and the period T) varies, the average primary productivity also varies. That is, primary productivity is sensitive to the duration of the individual upwelling events, even for constant T_a/T . The ecosystem has larger primary productivity if upwelling is fragmented into many episodes of short duration than if it happens during a few episodes of long duration, even though the total fraction of time during which the system experiences upwelling remains the same. Another quantity that varies with the value of T_a , for fixed T_a/T , is the residual nutrient concentration in the surface layer, N_{res} , defined as the nutrient that is not consumed by phytoplankton. For a restoring nutrient flux, the behavior of the residual nutrient concentration is similar to that of PP; see Figure 2b.

[16] To understand why primary productivity and residual nutrient concentration vary with the duration of the individual upwelling events, we must analyze in detail the properties of the nutrient-phytoplankton system. A first effect is the fundamental, and biologically sound, asymmetry between the short reaction time of phytoplankton growth to newly available nutrients ($1/\beta$ is about a day) and the longer mortality timescale for phytoplankton ($1/\mu_P$ is about a month). This asymmetry reflects the ability of plankton to survive for long times in nutrient-poor regions and to react quickly to the presence of nutrients when they become available.

[17] Additionally, attention should be paid to the fact that with a restoring nutrient flux, the nutrient flux is proportional to the difference between the deep water nutrient concentration N_0 and the mixed layer concentration N . Consumption by phytoplankton decreases the local nutrient concentration and consequently enhances the nutrient flux from deep water, partially counterbalancing nutrient depletion.

[18] The asymmetry in the relaxation rate of the nutrient is another, and most important, mechanism. At the beginning of an active phase, nutrient concentration in the surface layer relaxes from the low values present before the start of the active phase to the large values typical of intense upwelling. The opposite happens after a transition from an active to a low-productivity, normal phase. For simplicity, assume that the N , P , and Z fields are at their fixed points before the transition, and denote by N_a^* and N_n^* the fixed-point values for

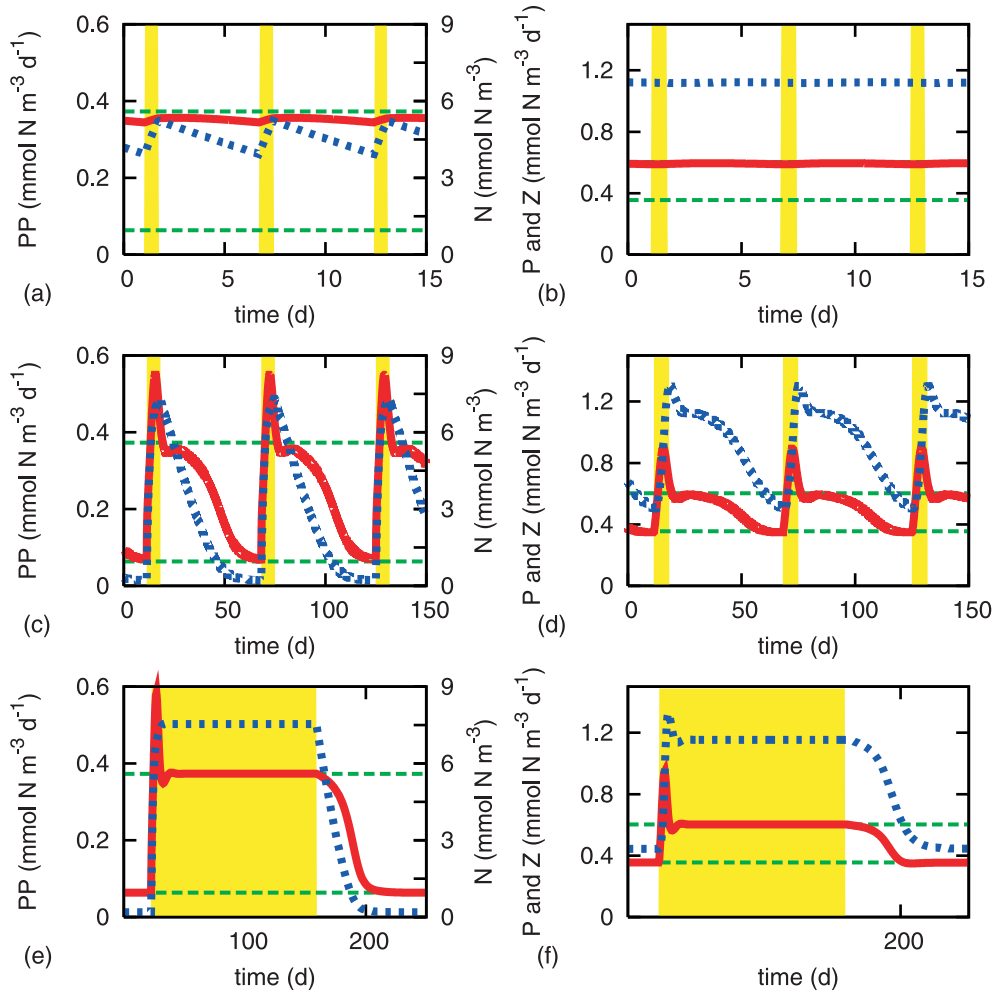


Figure 1. Ecosystem dynamics for a temporally varying, restoring nutrient flux. (left) Primary productivity (solid lines) and residual nutrient concentration (dark dashed lines). (right) Phytoplankton (solid lines) and zooplankton concentrations (dark dashed lines) as functions of time, for a fixed ratio $T_a/T = 0.12$ and for three different values of the duration of the active phases, (a, b) $T_a = 0.68d$, (c, d) $T_a = 6.8d$, and (e, f) $T_a = 136d$. Periods of strong upwelling are shaded. Light dashed horizontal lines indicate the steady state values of primary productivity, PP (Figures 1a, 1c, 1e) and of phytoplankton abundance, P (Figures 1b, 1d, 1f) corresponding to normal and active conditions.

the nutrient concentration corresponding to active and normal conditions, respectively. Immediately before a transition from a normal to an active phase, the nutrient flux is $S_n(N_0 - N_n^*)$, and it becomes $S_a(N_0 - N_n^*)$ immediately after the transition: The flux increases by $(S_a - S_n)(N_0 - N_n^*)$ at the transition. Similarly, the nutrient flux just before the transition from an active to a normal phase is $S_a(N_0 - N_a^*)$, and it is reduced to $S_n(N_0 - N_a^*)$ immediately after the transition: In this case, the flux variation at the transition is $(S_n - S_a)(N_0 - N_a^*) < 0$. Note that $N_a^* > N_n^*$ and therefore the decrease of the nutrient flux at the transition from active to normal conditions is smaller than the increase of the flux at the transition from normal to active conditions, $(S_a - S_n)(N_0 - N_a^*) < (S_a - S_n)(N_0 - N_n^*)$. The net effect of each pair of transitions is thus to increase the nutrient flux. If T_a is reduced, the number of transition pairs in a given time increases, and so does the nutrient flux.

[19] At very large values of T_a , all the relaxation time-scales of the ecosystem become negligible compared with

the duration of active and normal phases (Figure 1, bottom). In these adiabatic conditions, the mean PP saturates to the weighted average between the productivity experienced during active and normal phases, $PP_{ave} = (T_n PP_n + T_a PP_a)/T$, where PP_a and PP_n are the steady state primary productivities of a system which is constantly in active or normal phases respectively.

[20] As T_a is shortened for fixed T_a/T , the duration of the transients becomes comparable with the duration of the active or normal phases, and the asymmetry in the relaxation rates becomes significant. In particular, the duration of the intervals can become too short to allow the system to relax to the appropriate stationary solution (Figure 1, middle). As previously discussed, the system experiences a larger net nutrient input as the duration of active and normal phases is reduced. Interestingly, for very short values of T_a the system dynamics integrates over the rapid alternance between active and normal phases (Figure 1, top), and the productivity converges to that of an ecosystem

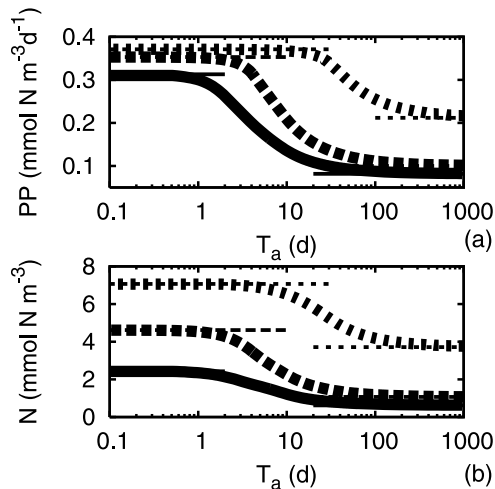


Figure 2. Relaxation nutrient flux. (a) Average primary productivity and (b) average residual nutrient concentration as a function of the duration of strong upwelling events, T_a . Different curves correspond to different values of T_a/T : 0.06 (solid line), 0.12 (long-dashed line), and 0.48 (short-dashed line). The thin horizontal lines on the left and on the right of the figure represent asymptotic values (see text for details).

with constant nutrient relaxation rate given by the weighted average of the rates during active and normal periods, $S_{ave} = (T_n S_n + T_a S_a)/T$, as shown by the thin horizontal lines on the left of Figure 2a. (See also *Claussen* [1995] for a discussion of a similar flux-aggregation problem in atmospheric models.) The residual nutrient concentration behaves similarly to primary productivity, and its dependence on T_a (for fixed T) simply reflects the fact that more nutrient is brought into the surface layer for smaller T_a , and not all of it can be immediately consumed by the phytoplankton.

[21] Note, finally, that the behavior observed here is not due to the periodic nature of the alternance between active and normal conditions, as similar results are obtained with non-periodic shifts between the two states. In this latter case, T , T_a , and T_n must be interpreted in terms of average quantities.

3.2. Fixed Nutrient Flux

[22] In the case of a fixed nutrient flux (FF), we assume the flux to be independent of the nutrient concentration in the mixed layer. Thus the feedback between consumption and nutrient flux is absent. In this case, the main asymmetry remaining is that related to the difference between the growth and death rates of phytoplankton.

[23] The flux is now defined as $\Phi_N = \Phi_n$ during normal conditions (of duration T_n), and $\Phi_N = \Phi_a$ during active phases (of duration T_a). The values chosen here for Φ_n and Φ_a correspond to the steady state restoring fluxes described previously, using S_n and S_a as relaxation rates. With these choices, the nutrient concentration in the surface layer never reaches the deep ocean value N_0 . Figure 3 shows the time evolution of N , P , and Z and of the primary productivity, PP , for three examples with $T_a/T = 0.12$ and $T_a = 0.68d$, $T_a = 6.8d$ and $T_a = 1360d$, respectively.

[24] In the FF case, for fixed T_a/T the amount of nutrient that is brought into the mixed layer does not vary with the

duration of the events, and the transitions between large and small nutrient flux are instantaneous. As a consequence, with this form of nutrient flux, despite the different temporal behavior of the nutrient concentration for different T_a (see Figure 3, left), the average primary productivity depends only on the ratio T_a/T , as indicated by Figure 4a. This can be understood by observing that the average rates of change of the concentrations on a period are $\langle dN/dt \rangle = \langle dP/dt \rangle = \langle dZ/dt \rangle = 0$. From the averaged equation for the nutrient concentration one gets $\langle PP \rangle (1 - \mu_N) = \langle \Phi_N \rangle$; that is, the average primary productivity depends only on the average nutrient flux.

[25] Despite the independence of primary productivity of the duration of the events, an interesting behavior for the residual nutrient concentration, N_{res} , emerges. For fixed T_a/T , the value of N_{res} depends on the duration of the individual upwelling events, T_a , as shown in Figure 4b. Opposite to what was observed for the restoring flux, larger values of T_a are now associated with larger residual nutrient concentration.

[26] The behavior of N_{res} can be understood by noticing that, with fixed-flux conditions, the average abundance of phytoplankton decreases for increasing values of T_a , as shown in Figure 4c. Owing to the asymmetry between growth and death rates of phytoplankton, the transition from low to high abundance during active phases is faster than the transition from high to low plankton abundance during normal phases. As a consequence, for values of T_a (and T_n) comparable to $1/\mu_B$, the average value of phytoplankton abundance during normal phases remains larger than it would be for a steady state system with low nutrient flux. Thus the average phytoplankton abundance becomes larger for smaller values of T_a . Since phytoplankton consumes nutrient, and the total nutrient input is fixed, more nutrient is consumed for small T_a and one observes smaller values of the residual nutrient concentration.

[27] For very short and very long active phases, the value of N_{res} saturates. The asymptotic value at short T_a is given by the steady state of a system with a constant nutrient flux given by the weighted average of the fluxes during active and normal phases, $\Phi_{ave} = (T_a \Phi_a + T_n \Phi_n)/T$ (horizontal lines on the left of Figure 4b; see also Figure 3, top, for the temporal dependence of the system). At large T_a (Figure 3, bottom), the system converges to the asymptotic state, given by the weighted average of the steady state nutrient concentrations during the two phases (adiabatic case, horizontal lines on the right of Figure 4b).

[28] Whenever the two types of flux are simultaneously present (as in the case of an upwelling event coupled with a wind-driven dust deposition episode), we did not detect any qualitatively new behavior. For a mixed flux, we found that the system response is intermediate between the two types of behavior found for pure RF and FF cases, and the detailed results depend on the relative importance of the two forms of nutrient input.

4. Effects of the Spatial Variability of Nutrient Fluxes

4.1. A Model for Horizontal Advection

[29] In many parts of the ocean, nutrient input is characterized by strong spatial variability and is often associated with mesoscale and sub-mesoscale flow structures, such as

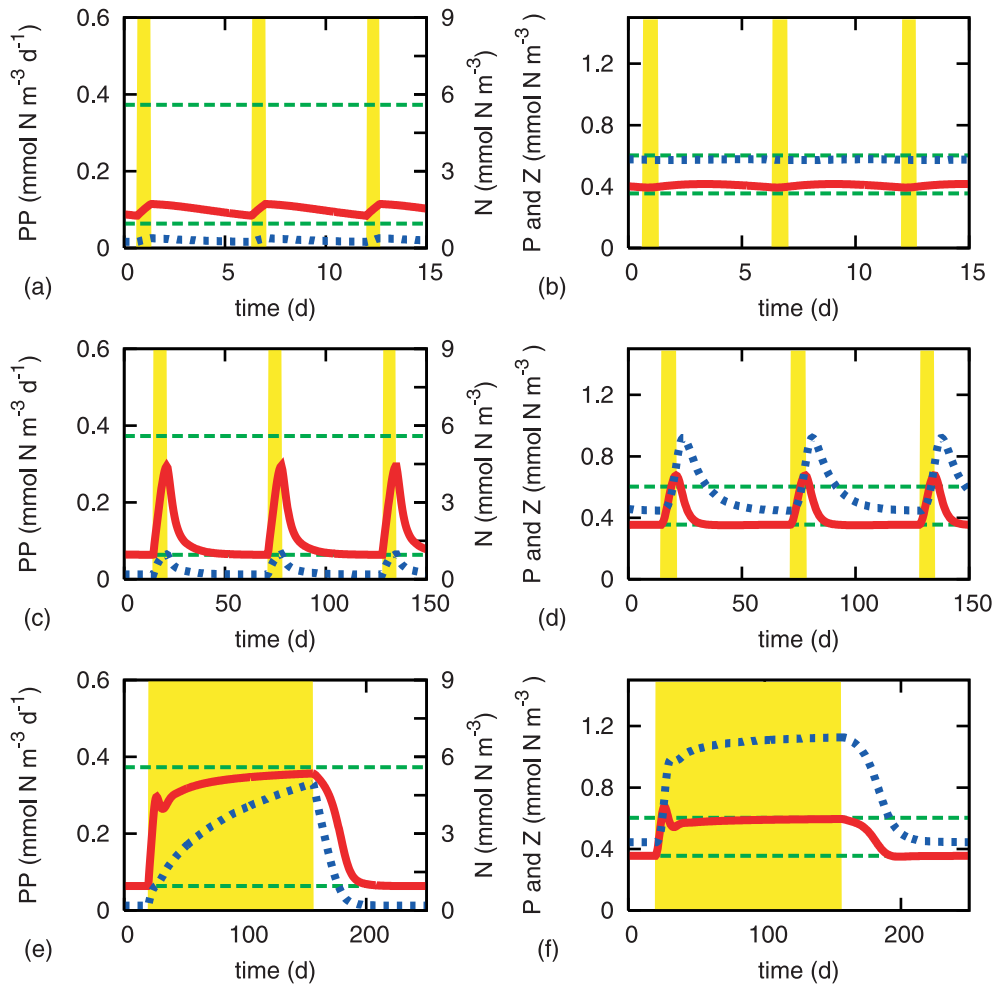


Figure 3. Ecosystem dynamics for a temporally varying, fixed-flux nutrient input. (left) Primary productivity (solid lines) and residual nutrient concentration (dark dashed lines). (right) Phytoplankton (solid lines) and zooplankton concentrations (dark dashed lines) as functions of time, for a fixed ratio $T_a/T = 0.12$ and for three different values of the duration of the active phases, $T_a = 0.68d$ (Figures 3a and 3b), $T_a = 6.8d$ (Figures 3c and 3d), $T_a = 1360d$ (Figures 3e and 3f). Periods of strong upwelling are shaded. Light dashed horizontal lines indicate the steady state values of primary productivity, PP (Figures 3a, 3c, 3e) and of phytoplankton abundance, P (Figures 3b, 3d, 3f) corresponding to normal and active conditions.

fronts, eddies, vortices, and filaments, that occur on spatial scales as small as a few kilometers and temporal scales as short as a few hours. Mesoscale advection processes and nutrient input variability can therefore occur on timescales that are of the same order of the planktonic reaction (growth) time, leading to significant interplay between physical and biological dynamics and to the lack of temporal scale separation between the different physical and biological processes.

[30] In order to resolve these scales in detail, we consider a barotropic quasigeostrophic (QG) turbulent flow, that we take as a first approximation to ocean mesoscale turbulence far from coastal boundaries [Salmon, 1998]. The choice of barotropic flow is dictated by the desire of keeping the horizontal advection model as simple as possible. The use of fully three-dimensional, baroclinic QG turbulence provides analogous results, since Lagrangian statistics in barotropic and baroclinic QG flows are very similar [Bracco *et al.*, 2004].

[31] The dynamics of incompressible, two-dimensional horizontal turbulent flows is described by a stream function ψ , and the fluid velocity, $\mathbf{u} = (u, v)$, is given by $u = -\partial_y \psi$ and $v = \partial_x \psi$, [see, e.g., Pedlosky, 1987]. The evolution equation for ψ is

$$\frac{\partial \nabla^2 \psi}{\partial t} + [\psi, \nabla^2 \psi] = D + F, \quad (5)$$

where $\nabla^2 \psi$ is relative vorticity, square brackets indicate the two-dimensional Jacobian operator, and D and F are dissipation and forcing terms, respectively. Dissipation is provided by the sum of a hyperviscosity term, $D_p = (-1)^{p-1} \nu_p \nabla^{2p} \nabla^2 \psi$, acting on small scales, and of a hypoviscosity term, $D_q = (-1)^{q-1} \nu_q \nabla^{-2q} \nabla^2 \psi$, that removes the energy accumulated at large scales by the inverse energy cascade typical of QG turbulence. Forcing is obtained by keeping the power spectrum fixed at a given wave number k_F , and allowing the Fourier phase at k_F to

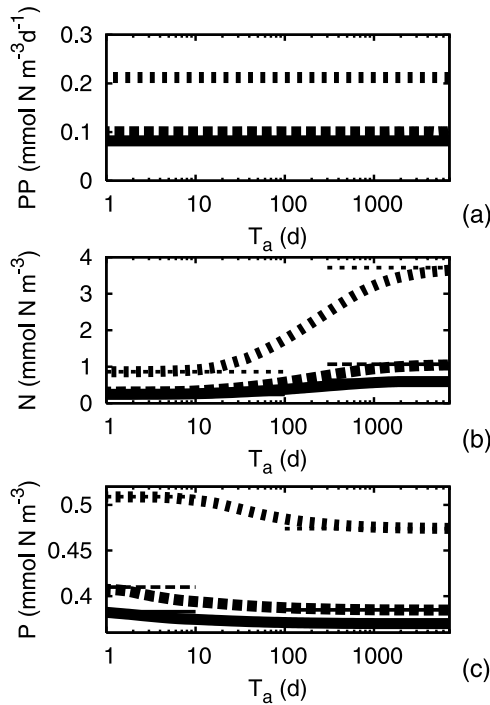


Figure 4. Fixed nutrient flux. (a) Average primary productivity, (b) average residual nutrient concentration, and (c) plankton abundance as functions of the duration of the active phases, T_a , when the nutrient flux is independent of the nutrient concentration (FF, fixed flux case). Different lines refer to different values of T_d/T_a : $T_d = 0.06T$ (solid line), $T_d = 0.12T$ (long-dashed line), and $T_d = 0.48T$ (short-dashed line).

evolve dynamically. In this way, a statistically stationary state can be achieved [Babiano *et al.*, 1987]. The equation of motion (5) is integrated numerically in a doubly periodic square domain which represents a portion of the open ocean, using a pseudo-spectral code and a third-order Adams-Bashforth time integration scheme. The spatial resolution is 2 km and the square domain has side 1024 km. The robustness of the results has been tested by repeating some of the integrations in a smaller domain with spatial resolution of 0.5 km.

[32] One of the main properties of quasigeostrophic turbulence is the presence of energetically dominant, long-lived coherent vortices, which are surrounded by regions of strong shear and by vorticity filaments that originate from vortex-vortex interactions [McWilliams, 1984, 1990; Bracco *et al.*, 2000, 2004]. On average, the statistically stationary turbulent flow we consider in this study is populated by about 120 vortices with average radius of 14 km, mean eddy turnover time of 3 days, and r.m.s. velocity fluctuations of $\sigma = 10$ cm/s. (When nutrient input regions are not correlated with flow structures, the only crucial quantities are the turbulent eddy kinetic energy and the eddy Lagrangian integral time, and the details of the eddy field do not affect the results presented here. Changes in the average size of the vortices induce quantitative changes in PP estimates when the nutrient input is associated with the eddies, due to the trapping properties of the vortex cores.)

[33] In the following, we assume that all biological fields (nutrient, phytoplankton, and zooplankton) are passively

advected by the same turbulent flow, obtained by integrating numerically the barotropic QG equation. The evolution equations for the ecosystem become

$$\begin{cases} \frac{\partial N}{\partial t} + [\psi, N] = f(N, P, Z), \\ \frac{\partial P}{\partial t} + [\psi, P] = g(N, P, Z), \\ \frac{\partial Z}{\partial t} + [\psi, Z] = h(N, P, Z), \end{cases} \quad (6)$$

where we ignore direct diffusion of biological fields. At the scales we consider here, diffusion of biological tracers plays a limited role and the dominant effect is the explicit spatial advection by mesoscale turbulence. Numerical integration of the ecosystem equations is performed by a semi-Lagrangian method (see Appendix A and Pasquero *et al.* [2004] for details).

[34] The nutrient input is assumed to be spatially inhomogeneous, with active regions of strong nutrient flux surrounded by oligotrophic ambient waters, similar to the configuration adopted by Martin *et al.* [2002]. The active regions are an ensemble of N_{patch} circular patches with radius R . The position of the patches is fixed in time, while plankton and nutrients are advected across the active regions by the turbulent flow. In the following, we consider seven different cases characterized by different values of R and N_{patch} , chosen so that the total area characterized by strong nutrient flux is kept constant, $A^2 = \sum_{N_{patch}} \pi R^2 = 0.12 L^2$ where L is the linear domain size. The cases considered range from one large patch of radius 200 km to 4096 regularly spaced patches with radius of about 3 km. A list of the configurations considered and of their identification number is given in Table 2.

[35] Figure 5 shows a snapshot of the fields of nutrient, phytoplankton and zooplankton in statistically stationary conditions for the case with 16 active regions, each having radius $R = 50$ km (case FF3). The largest concentration of phytoplankton is found in regions where the zooplankton concentration is small; in these regions, the nutrient concentration is depleted by the large consumption. Where the zooplankton concentration is large, phytoplankton abundance is significantly limited by zooplankton grazing and larger quantities of nutrient can accumulate. As a consequence of this interplay between phytoplankton and nutrient abundances, primary productivity (Figure 5d) is spatially more homogeneous than the individual N and P fields.

[36] In the above configurations, the nutrient input regions are not correlated with specific mesoscale flow

Table 2. Number and Radius of the Patches Characterized by Strong Nutrient Flux, in the Eight Configurations Considered

Configuration	Patch	Radius
1	$N_{patch} = 1$	$R = 200$ km
2	$N_{patch} = 4$	$R = 100$ km
3	$N_{patch} = 16$	$R = 50$ km
4	$N_{patch} = 64$	$R = 25$ km
5	$N_{patch} = 256$	$R = 12.5$ km
6	$N_{patch} = 1024$	$R = 6.25$ km
7	$N_{patch} = 4096$	$R = 3.12$ km
8	$N_{patch} \sim 120$	$\langle R \rangle \sim 18$ km

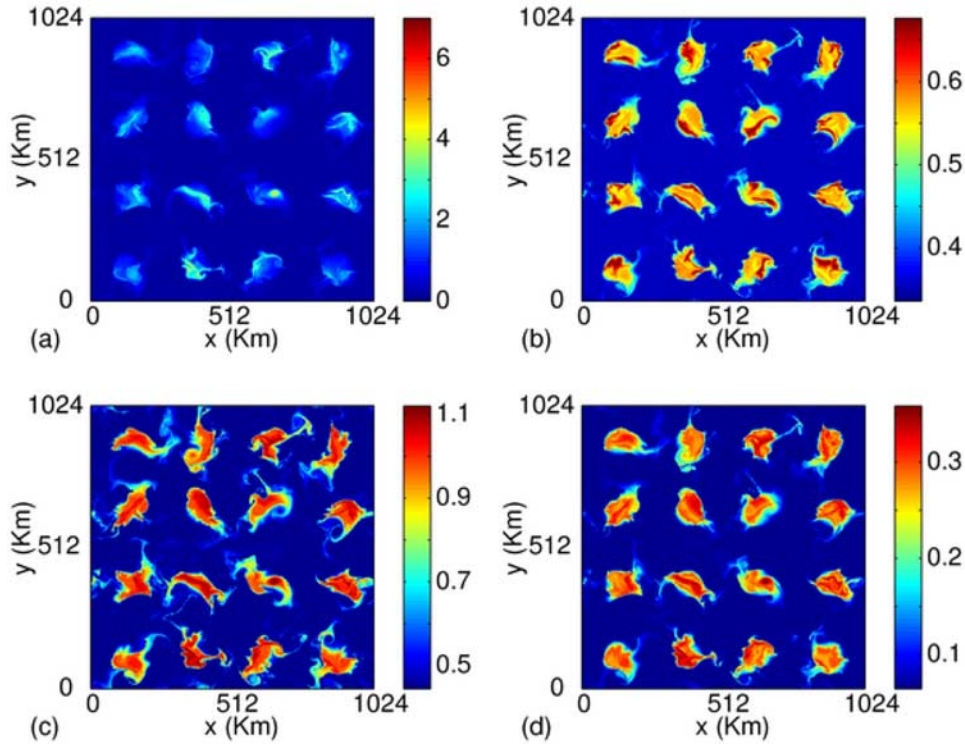


Figure 5. Snapshot of the (a) nutrient, (b) phytoplankton, (c) zooplankton, and (d) primary productivity for the run FF3, after statistically stationary conditions have been reached. Units are mmol N m^{-3} for nutrient, phytoplankton, and zooplankton concentrations, and $\text{mmol N m}^{-3} \text{d}^{-1}$ for primary productivity.

structures. Observational evidence suggests that nutrient input in the oceanic mixed layer is sometimes correlated with the vorticity field [McGillicuddy and Robinson, 1997; Oschlies and Garcon, 1998; Lévy et al., 2001; Lévy, 2003; Lévy and Klein, 2004]. To represent such a situation, we follow Martin et al. [2002] and consider one more configuration, identified as run 8, in which strong nutrient fluxes are confined in and around vortices. Also, in this case the total area of strong nutrient flux is about 12% of the domain area. For run 8, the average radius of individual upwelling regions, is $\langle R \rangle = 18 \text{ km}$, slightly larger than the average size of the vortex cores.

[37] After a transient that depends on the initial distribution of the biological fields, the system reaches a statistically stationary state. We first describe the ecosystem response in statistically stationary conditions, when domain-averaged quantities are approximately constant, and then we briefly examine the transient behavior.

4.2. Statistically Stationary Conditions: Restoring Nutrient Flux

[38] For restoring nutrient flux, primary productivity significantly depends on the size of nutrient patches, as shown in Figure 6a. The increased productivity in the case of many small active regions is due to a larger nutrient input compared to that found for fewer and larger active regions. Nutrient input is associated with the advection of ambient water into active regions, where it becomes enriched very rapidly. Nutrient consumption by phytoplankton further enhances the nutrient input, and primary productivity grows rapidly. Conversely, nutrient-rich waters advected into oligotrophic regions take a

longer time to become depleted as the large nutrient concentration relaxes slowly to the low values typical of normal conditions. The average concentration of available nutrients follows the change in the mean flux, and it increases with decreasing R , as shown in Figure 6b.

[39] The mechanism responsible for the enhancement of primary productivity for spatially fragmented active upwell-

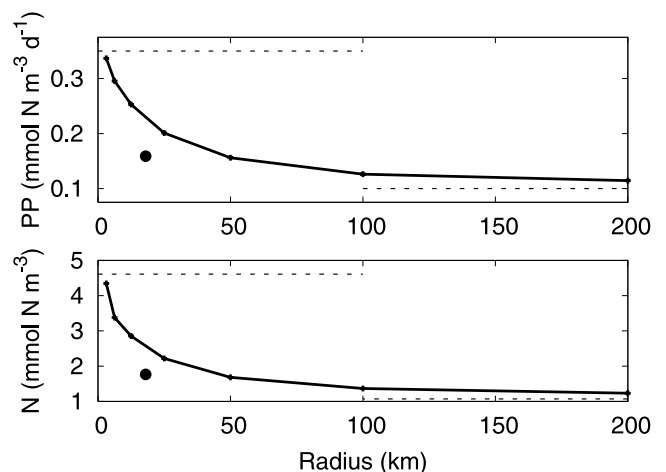


Figure 6. (top) Domain-averaged primary productivity and (bottom) domain-averaged residual nutrient concentration as functions of the size of individual active regions in the RF case. Thin dashed horizontal lines indicate the two asymptotic values at large and small values of R discussed in the text. Solid points indicate the values obtained when strong upwelling is correlated with the eddy field (run RF8).

ing regions relies on the fact that even for temporally persistent but spatially varying upwelling conditions, horizontal advection moves fluid parcels around, and each parcel experiences a temporally intermittent nutrient flux. (We assume that the nutrient input regions have fixed location, while the surface mixed layer water has horizontal motion. If there was no relative motion between the fluid parcels and the nutrient input regions, the nutrient flux had no time dependence, and the same diffusion was affecting nutrients and plankton, the effects discussed in this paper would disappear. However, it is enough that any of the above assumptions is not valid to induce the types of behavior discussed in this work. In the runs where the nutrient input regions are associated with the vortices, part of the nutrient input takes place around the vortex cores, where fluid particles are swept around by the turbulent velocity field.) If we neglect phytoplankton diffusion, a given fluid parcel containing phytoplankton is advected past active and normal regions (note that we consider fluid parcel with a horizontal size comparable with the numerical resolution of 2 km, and thus direct phytoplankton diffusion is negligible). Since the turbulent flow is statistically homogeneous and isotropic, the phytoplankton contained in a given fluid parcel will experience an alternance between active and normal conditions.

[40] The dependence on the spatial size of individual upwelling regions can thus be understood from the results on the temporal variability of the nutrient flux. Averaging over long times, and assuming that each fluid parcel explores uniformly the flow domain (as assured by the incompressibility and homogeneity of the advecting flow), we can estimate the total fraction of time spent in active regions from the fractional area covered by active regions, A^2/L^2 . For a fixed value of this total fractional area, the smaller the radius of the individual active regions (i.e., the more fragmented are the active areas), the shorter the duration of the individual events during which the phytoplankton in each fluid parcel experiences intense nutrient flux. The behavior found in this case is analogous to what we observed for a homogeneous system when the duration of the individual upwelling events decreases: Primary productivity increases for decreasing duration of the individual upwelling events, that is, for smaller size of the individual upwelling regions.

[41] For large radii of the individual upwelling regions, primary productivity tends to the weighted average of the steady state productivities in active and normal regions, $PP_{ave} = [A^2 PP_a + (L^2 - A^2) PP_n]/L^2$. In the limit of small upwelling regions, an estimate of primary productivity is provided by the steady state PP that would be observed for a system with a nutrient relaxation rate given by the area-weighted average of the relaxation rates in active and normal regions.

[42] Since coherent vortices act as transport barriers, correlations between the active regions of intense nutrient flux and the eddy field reduce the fluid parcel exchanges between active and oligotrophic regions [Provenzale, 1999; Martin *et al.*, 2002]. In fact, the primary productivity measured in run RF8 (where active regions are located in and around the vortices) is lower than that estimated for active patches with the same size of the vortices but uncorrelated from the eddy field [Martin *et al.*, 2002].

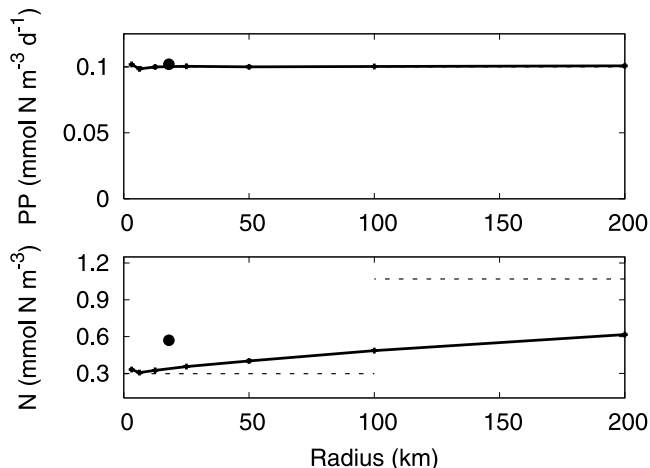


Figure 7. (top) Domain averaged primary productivity and (bottom) residual nutrient concentration, as functions of the size of active regions in the fixed-flux case. Solid points indicate the values obtained when the active regions are concentrated in and around vortices (run FF8). Horizontal dashed lines indicate the asymptotic values at large and small values of R , as discussed in the text.

The primary productivity for nutrient input in and around vortices is equivalent to that obtained for circular patches with radius of 50 km, a value which is 3 times larger than the average size of the patches correlated with the eddies.

4.3. Statistically Stationary Conditions: Fixed Nutrient Flux

[43] For fixed-flux nutrient input, the behavior of the spatially inhomogeneous system is again similar to that observed in the case of temporal variability of the nutrient supply, and the domain-averaged PP is independent of the size of the active regions; see Figure 7a.

[44] The average nutrient concentration in the surface layer increases for large areas of the active regions. For small values of R , the residual nutrient concentration converges to that obtained for a system that experiences a homogeneous nutrient flux given by the area-weighted average of the fluxes in active and normal regions (dashed horizontal line on the left of Figure 7b). As R increases, the average residual nutrient concentration becomes larger, and it is bounded by the asymptotic value obtained by the area-weighted average of the residual nutrient concentration (dashed horizontal line on the right of Figure 7b).

4.4. Transient Behavior

[45] We now consider the transient response of the ecosystem to a sudden nutrient input. The nutrient flux is switched on in different regions, defined as before, starting from the steady state corresponding to normal, low-nutrient conditions.

[46] Figure 8 shows the domain-averaged primary productivity during the first few weeks after the onset of the strong nutrient input event, for both RF and FF. In line with the results of the previous section, we observe that different functional forms of the nutrient flux lead to different results.

[47] In the restoring flux case, nutrient consumption by phytoplankton and horizontal advection cause a larger

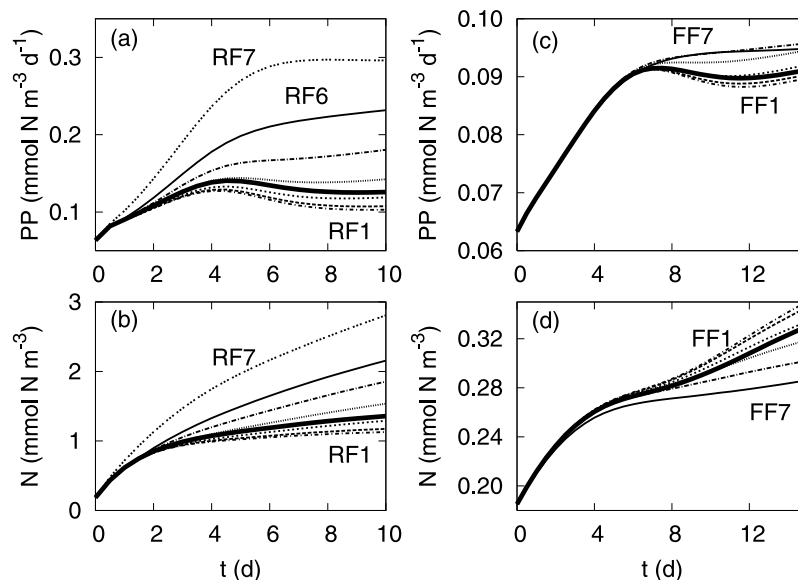


Figure 8. (a, c) Primary productivity and (b, d) residual nutrient concentration averaged over the domain in the first days after the onset of the active phase, starting from a homogeneous steady state corresponding to normal conditions. Different lines refer to different configurations of the active regions; thick solid lines indicate run 8. Nutrient is injected as a (Figures 8a and 8b) restoring flux and (Figures 8c and 8d) fixed flux.

nutrient input, inducing a much larger primary productivity and large residual nutrient concentrations as the size of the active regions is reduced. The behavior of the residual nutrient concentration is similar to that of primary productivity, and it becomes larger when the size of the active regions becomes smaller. In the fixed-flux case, primary productivity grows after switching on the nutrient flux, and at late times it tends to a value that is independent of the radius of the active regions. The residual nutrient concentration increases for increasing size of the individual active regions. For both RF and FF conditions, results are consistent with what is obtained in the statistically stationary state.

5. Discussion and Conclusions

[48] We have explored how the spatial and temporal variability of the nutrient input affects primary productivity and residual nutrient concentrations in the marine ecosystem. We did so by investigating the response of a simple NPZ ecosystem model, coupled to an advection flow model assumed to represent ocean mesoscale turbulence in the surface mixed layer, to temporally and/or spatially varying nutrient fluxes. The advecting flow is two-dimensional, and the vertical nutrient fluxes are externally imposed. Owing to lack of resolution in the vertical, the ecosystem model adopted does not have any explicit light limitation. The nutrient flux has been parameterized by either a restoring flux, taken to represent vertical turbulent mixing during upwelling events, or a fixed flux, assumed to represent nutrient input events that do not depend on the nutrient concentration in the surface layer, or by a combination of both.

[49] Our results indicate that the ecosystem response to the addition of nutrient depends on the spatial and temporal

variability of the nutrient flux, and not merely on its mean value. In addition, we found that the choice of the form of the nutrient flux (restoring versus fixed-flux) is a delicate issue as different, even opposite, ecosystem responses characterize the two cases.

[50] In a homogeneous ecosystem, the temporal variability of the nutrient flux can induce changes in the primary productivity for the restoring flux case, as discussed in section 3. For inhomogeneous conditions and in the presence of horizontal advection, the same results can be obtained by advecting fluid parcels containing the biological fields past active upwelling regions. The finite time during which a given fluid parcel experiences strong nutrient flux depends on the size of the active regions and on the average advection velocity. For a given advective flow, the smaller the active regions, the shorter the time spent by fluid parcels in individual active regions. Therefore the behavior of an ecosystem subject to spatially inhomogeneous upwelling coupled with horizontal advection can be interpreted in terms of an ecosystem homogeneous in space but subject to temporally intermittent upwelling events. For simplicity, we have considered spatially variable but temporally permanent upwelling areas. A full spatiotemporal variability of the active regions can only enhance the effect discussed here.

[51] The results we presented indicate that the strong variability of the diapycnal diffusivity observed in the ocean [Ledwell and Hickey, 1995; Ledwell et al., 2000], and the isopycnal mixing associated with frontal and submesoscale dynamics, can significantly increase the nutrient fluxes when coupled to horizontal advection. The mechanism relies on the removal of nutrients from the active regions by horizontal advection on timescales shorter than the phytoplankton doubling time. This allows for the maintenance of large nutrient fluxes. There are indications that in

coastal regions, where the input is associated to Ekman pumping, the bloom develops offshore, because of the currents that advect the nutrient away from the coast before the phytoplankton can reproduce and grow [Boyd and Smith, 1983; Gargett and Marra, 2002].

[52] Sarmiento *et al.* [2004] have recently shown that a large portion of the nutrient input into the subtropical gyres is upwelled in the Southern Ocean, and then advected at the base of the main thermocline at low latitudes, where wind-driven turbulence can reach it and bring it into the euphotic layer. Their analysis highlights the importance of isopycnal advection combined with inhomogeneous upwelling on large scales. Our study suggests that horizontal advection can be important also at small scales, when combined with inhomogeneities in the nutrient sources to the surface layer. Interestingly, if the upwelling is associated with coherent vortices we find a lower primary productivity, due to the trapping properties of the vortices and the limited water exchanges between the vortex cores and the surrounding fluid. Correlations between vertical and horizontal velocities can thus play a very important role in determining primary productivity.

[53] One implication of this study is that estimates of primary productivity by ocean circulation models can be erroneous if a restoring nutrient flux is assumed and the mesoscale and submesoscale fragmentation of the upwelling regions is not properly resolved. If a coarse resolution model includes a few large active areas of strong upwelling instead of many smaller active areas, primary productivity can be significantly underestimated, consistent with the results of Martin *et al.* [2002]. The estimated productivity is close to the area-weighted average of the steady state productivities, which provides only a lower bound to primary productivity. On the other hand, we found that the estimate of the steady state primary productivity for a system which has a nutrient relaxation rate given by the area-weighted average of the relaxation rates in active and normal regions provides an approximate upper bound to the true primary productivity. This suggests that in coarse resolution models, one could bracket primary productivity estimates by evaluating both the area-weighted PP and the steady state PP corresponding to the area-weighted value of the vertical relaxation rate in active and normal regions.

[54] Our study also indicates that with fixed-flux nutrient input, high-nutrient, low-chlorophyll (HNLC) regions can appear without modifying the mean nutrient input nor the primary productivity, as a result of episodes of nutrient input of long duration and/or of large spatial extent. The ecosystem becomes more efficient at consuming nutrients as the number (or the fractionation) of nutrient injection events increases. In spatially inhomogeneous conditions, low horizontal mixing can also induce the formation of HNLC regions. Recently, Platt *et al.* [2003] associated HNLC regions to changes in mixed layer depth, without the need for micronutrient limitation, and suggested light to be the limiting factor. Our results, on the other hand, indicate that even if nutrients and light are abundant, HNLC regions can nevertheless appear.

[55] We also found that the response of the ecosystem to the fragmentation of the nutrient input can be very sensitive to the parameterization used to describe nutrient

fluxes. In particular, we found an opposite behavior of the residual nutrient concentration as a function of the size of the active regions for restoring or fixed-flux nutrient input.

[56] The major limitations of this study are that the nutrient fluxes are imposed externally, and that light limitation is not taken into account. This indicates that a better representation of nutrient fluxes is needed: Fluxes associated with dynamical, three-dimensional processes should be carefully studied and quantified by advection models capable of representing the correlations between vertical and horizontal velocities. Three-dimensional models of ocean flows and more complex, multicompartment ecosystem models, able to account for the competition between different phytoplankton species, will be used to further advance this study.

Appendix A

[57] The numerical integration of advection-reaction-diffusion equations is associated with nontrivial problems, related to the formation of sharp fronts that can destabilize the solution, and to the appearance of physically unrealistic, negative values for the concentrations. Usually, these problems can be overcome by introducing large values of the diffusion coefficients and/or schemes that smooth away large gradients [Smolarkiewicz and Margolin, 1998; Zalesak, 1979; Hourdin and Armengaud, 1999]. However, sharp edges and fronts are certainly present in the chlorophyll and nutrient concentration fields in the ocean. The elimination of these gradients is particularly inappropriate as frontal regions are often associated with large primary productivity. Thus integration schemes capable of resolving strong gradients are needed.

[58] To integrate the ecosystem equations, we assume that the biological fields do not affect the fluid dynamics (i.e., they are passive tracers), and we adopt a semi-Lagrangian scheme that separates the advection and reaction parts in the evolution equation for the biological fields. First, we numerically integrate, on an Eulerian grid, the evolution equations for the velocity field $\mathbf{u} \equiv (u, v)$. This velocity field is then used to obtain Lagrangian trajectories of a large number of fluid parcels, by integrating the Lagrangian equations

$$\frac{d\mathbf{X}_i}{dt} = \mathbf{u}(\mathbf{X}_i, t), \quad (\text{A1})$$

where $\mathbf{X}_i(t) \equiv [X_i(t), Y_i(t)]$ is the position of the i th parcel at time t and the velocity field \mathbf{u} is evaluated at the parcel position. Each parcel represents a given water volume (taken to have the size of the grid cells used to integrate the Eulerian momentum equations), and it is assumed to have homogeneous properties. Each parcel is characterized by a concentration of the three fields N , P , and Z , which vary in time accordingly to the ecosystem equations for a homogeneous system. That is, biogeochemical reactions occur within each parcel, and do not depend on the concentration of biogeochemical fields in neighboring parcels. The ecosystem fields are then obtained by interpolating the concentrations provided by the ensemble of water parcels onto a regular grid. The

inclusion of a diffusion term can be accounted for by introducing mixing among nearby water parcels [Pasquero *et al.*, 2004]. In the present study, we do not include mixing between neighboring parcels.

[59] This method, used by Abraham [1998] in the case of a synthetic velocity field generated by a random distribution of circular eddies, allows for computing the Lagrangian trajectories once and for all. The ecosystem model can then be integrated along these trajectories, with very low computational cost. Therefore this method is particularly suited for an extensive study of different formulations of the ecosystem model in the same advecting flow.

[60] The semi-Lagrangian method is more easily applied to nondivergent flows; otherwise, accumulation of Lagrangian fluid parcels into convergence regions and rarefaction of the particle concentration in divergence regions can lead to a spatially variable resolution in the biological fields. For nondivergent flows such as those considered here, fluctuations in the fluid parcel distribution are due only to Poisson noise.

[61] In our simulations, Lagrangian trajectories are initialized on a regular grid that covers the whole domain and coincides with the grid used to integrate the Eulerian momentum equation, for a total of 262,144 water parcels. Lagrangian velocities are calculated from the Eulerian field at the position of the fluid parcels, using a cubic spline interpolation scheme. Owing to the large number of parcels used in this study, fluctuations in the Lagrangian parcel concentration are very small. In the present simulations, for any given parcel the closest neighbor is located within two grid points, and the number of water parcels per cell is larger than 2 in less than 5% of the cells. For a direct comparison of the concentration fields obtained with the semi-Lagrangian approach and with the direct integration of the advection-reaction-diffusion Eulerian equations of the ecosystem model, the reader is referred to Pasquero *et al.* [2004].

[62] **Acknowledgments.** We are grateful to Miro Gacic for showing us the relevance of this work to the Mediterranean Sea, and to two anonymous referees for their valuable comments and suggestions. This work was partially supported by the EU contract HPRN-CT-2002-00300 "Fluid Mechanical Stirring and Mixing: The Lagrangian Approach."

References

- Abraham, E. (1998), The generation of plankton patchiness by turbulent stirring, *Nature*, *391*, 577–580.
- Babiano, A., C. Basdevant, P. le Roy, and R. Sadourmy (1987), Single-particle dispersion, Lagrangian structure function and Lagrangian energy spectra in two-dimensional incompressible turbulence, *J. Mar. Res.*, *45*, 107–131.
- Boyd, C., and S. Smith (1983), Plankton, upwelling and coastally trapped waves off Peru, *Deep Sea Res.*, *30*, 723–742.
- Bracco, A., J. McWilliams, G. Murante, A. Provenzale, and J. Weiss (2000), Revisiting freely decaying two-dimensional turbulence at millennial resolution, *Phys. Fluids*, *12*, 2931–2941.
- Bracco, A., J. von Hardenberg, A. Provenzale, J. B. Weiss, and J. McWilliams (2004), Dispersion and mixing in quasigeostrophic turbulence, *Phys. Rev. Lett.*, *92*, doi:084501.
- Claussen, M. (1995), Flux aggregation at large scales: On the limits of validity of the concept of blending height, *J. Hydrol.*, *166*, 371–382.
- Doney, S., et al. (2004), Evaluating global ocean carbon models: The importance of realistic physics, *Global Biogeochem. Cycles*, *18*, GB3017, doi:10.1029/2003GB002150.
- Edwards, A., and J. Brindley (1996), Oscillatory behaviour in a three-component plankton population model, *Dyn. Stability Syst.*, *11*, 347–370.
- Edwards, A., and A. Yool (2000), The role of higher predation in plankton population models, *J. Plankton Res.*, *22*, 1085–1112.
- Falkowski, P., D. Ziemann, Z. Kolber, and P. Bienfang (1991), Role of eddy pumping in enhancing primary production in the ocean, *Nature*, *352*, 55–58.
- Fasham, M. (1993), Modelling the marine biota, in *The Global Carbon Cycle*, edited by M. Heimann, pp. 457–504, Springer, New York.
- Fasham, M., H. Ducklow, and S. McKelvie (1990), A nitrogen-based model of plankton dynamics in the oceanic mixed layer, *J. Mar. Res.*, *48*, 591–639.
- Gargett, A., and J. Marra (2002), Effects of upper ocean physical processes (turbulence, advection and air-sea interaction) on oceanic primary production, in *The Sea*, vol. 12, edited by A. Robinson, J. McCarthy, and B. Rothschild, pp. 19–49, John Wiley, Hoboken, N. J.
- Hourdin, F., and A. Armgand (1999), The use of finite-volume methods for atmospheric advection of trace species: Part I. Test of various formulations in a general circulation model, *Mon. Weather Rev.*, *127*, 822–837.
- Jenkins, W. (1988), Nitrate flux into the euphotic zone near Bermuda, *Nature*, *331*, 521–523.
- Jenkins, W., and S. Doney (2003), The subtropical nutrient spiral, *Global Biogeochem. Cycles*, *17*(4), 1110, doi:10.1029/2003GB002085.
- Kot, M. (2001), *Elements of Mathematical Ecology*, Cambridge Univ. Press, New York.
- Ledwell, J., and B. Hickey (1995), Evidence for enhanced boundary mixing in the Santa Monica basin, *J. Geophys. Res.*, *100*, 20,665–20,679.
- Ledwell, J., E. Montgomery, K. Polzin, L. S. Laurent, R. Schmitt, and J. Toole (2000), Evidence for enhanced mixing over rough topography in the abyssal ocean, *Nature*, *403*, 179–182.
- Lévy, M. (2003), Mesoscale variability of phytoplankton and of new production: Impact of the large-scale nutrient distribution, *J. Geophys. Res.*, *108*(C11), 3358, doi:10.1029/2002JC001577.
- Lévy, M., and P. Klein (2004), Does the low frequency variability of mesoscale dynamics explain a part of the phytoplankton and zooplankton spectral variability?, *Proc. R. Soc. London, Ser. A*, *460*, 1673–1687.
- Lévy, M., P. Klein, and A.-M. Treguier (2001), Impact of sub-mesoscale physics on production and subduction of phytoplankton in an oligotrophic regime, *J. Mar. Res.*, *59*, 535–565.
- Mahadevan, A., and D. Archer (2000), Modeling the impact of submesoscale circulation on the nutrient supply and biogeochemistry of the upper ocean, *J. Geophys. Res.*, *105*(C1), 1209–1225.
- Mahaffey, C., R. Williams, and G. Wolff (2004), Physical supply of nitrogen to phytoplankton in the Atlantic Ocean, *Global Biogeochem. Cycles*, *18*, GB1034, doi:10.1029/2003GB002129.
- Martin, A., K. Richards, and M. Fasham (2001), Phytoplankton production and community structure in an unstable frontal region, *J. Mar. Syst.*, *28*, 65–89.
- Martin, A., K. Richards, A. Bracco, and A. Provenzale (2002), Patchy productivity in the open ocean, *Global Biogeochem. Cycles*, *16*(2), 1025, doi:10.1029/2001GB001449.
- McGillicuddy, D. J., and A. Robinson (1997), Eddy-induced nutrient supply and new production in the Sargasso Sea, *Deep Sea Res., Part I*, *44*, 1427–1450.
- McWilliams, J. (1984), The emergence of isolated coherent vortices in turbulent-flow, *J. Fluid Mech.*, *146*, 21–43.
- McWilliams, J. (1990), The vortices of two-dimensional turbulence, *J. Fluid Mech.*, *219*, 361–385.
- Oschlies, A., and V. Garçon (1998), Eddy-induced enhancement of primary production in a model of the North Atlantic Ocean, *Nature*, *394*, 266–269.
- Oschlies, A., and V. Garçon (1999), An eddy-permitting coupled physical-biological model of the North Atlantic: 1. Sensitivity to advection numerics and mixed layer physics, *Global Biogeochem. Cycles*, *13*, 135–160.
- Pasquero, C., A. Bracco, and A. Provenzale (2004), Coherent vortices, Lagrangian particles and the marine ecosystem, in *Shallow Flows*, edited by G. Jirka and W. Uijtewaal, pp. 399–412, A. A. Balkema, Brookfield, Vt.
- Pedlosky, J. (1987), *Geophysical Fluid Dynamics*, Springer, New York.
- Platt, T., D. Broomhead, S. Sathyendranath, A. Edwards, and E. Murphy (2003), Phytoplankton biomass and residual nitrate in the pelagic ecosystem, *Proc. R. Soc. London, Ser. A*, *459*, 1063–1073.
- Provenzale, A. (1999), Transport by coherent barotropic vortices, *Ann. Rev. Fluid Mech.*, *31*, 55–93.
- Salmon, R. (1998), *Lecture Notes on Geophysical Fluid Dynamics*, Oxford Univ. Press, New York.
- Sarmiento, J., N. Gruber, M. Brzezinski, and J. Dunne (2004), High-latitude controls of thermocline nutrients and low latitude biological productivity, *Nature*, *427*, 56–60.

- Siegel, D., D. J. McGillicuddy Jr., and E. Fields (1999), Mesoscale eddies, satellite altimetry, and new production in the Sargasso Sea, *J. Geophys. Res.*, *104*(C6), 13,359–13,379.
- Smolarkiewicz, P., and L. Margolin (1998), MPDATA: A finite difference solver for geophysical flows, *J. Comput. Phys.*, *140*, 459–480.
- Steele, J., and E. Henderson (1992), The role of predation in plankton models, *J. Plankton Res.*, *14*, 157–172.
- Truscott, J., and J. Brindley (1994), Equilibria, stability and excitability in a general class of plankton population models, *Philos. Trans. R. Soc. London, Ser. A*, *347*, 703–718.
- Williams, R., and M. Follows (2003), Physical transport of nutrients and the maintenance of biological production, in *Ocean Biogeochemistry: The Role of the Ocean Carbon Cycle in Global Change*, edited by M. Fasham, pp. 19–51, Springer, New York.
- Zalesak, S. T. (1979), Fully multidimensional flux-corrected transport algorithms for fluids, *J. Comput. Phys.*, *31*, 335–362.
-
- A. Bracco, Physics of Weather and Climate Group, Abdus Salam International Center for Theoretical Physics, Strada Costiera 11, I-34100 Trieste, Italy. (annalisa@ictp.it)
- C. Pasquero, Geological and Planetary Sciences Division, California Institute of Technology, MC 100-23, 1200 E. California Boulevard, Pasadena, CA 91125, USA. (claudia@gps.caltech.edu)
- A. Provenzale, Istituto di Scienze dell'Atmosfera e del Clima, Consiglio Nazionale delle Ricerche, corso Fiume 4, I-10133 Torino, Italy. (a.provenzale@isac.cnr.it)